# Rendering Discrete Participating Media with Geometrical Optics Approximation

## APPENDIX A
## A BRIEF INTRODUCTION OF LORENZ-MIE THEORY

In this section, we briefly describe Lorenz-Mie theory [1], [2] which has already been employed in computer graphics [3], [4], [5], [6], [7]. For light scattering of an electromagnetic wave from a homogeneous spherical particle, exact solutions of the two scattering amplitude functions $S_1$ and $S_2$ are given by:

$$S_1(\theta, r) = \sum_{n=1}^{\infty} \frac{2n+1}{n(n+1)} [a_n(r)\pi_n(\cos\theta) + b_n(r)\tau_n(\cos\theta)] \tag{26}$$

$$S_2(\theta, r) = \sum_{n=1}^{\infty} \frac{2n+1}{n(n+1)} [b_n(r)\pi_n(\cos\theta) + a_n(r)\tau_n(\cos\theta)] \tag{27}$$

which express the scattered fields in terms of an infinite series of spherical multipole partial waves. Here, $a_n(r)$ and $b_n(r)$ are the Lorenz-Mie coefficients of particle size $r$; $\pi_n(\cos\theta)$ and $\tau_n(\cos\theta)$ are derived from the Legendre functions. Please refer to [7] for the details and the expressions of $a_n(r)$, $b_n(r)$, $\pi_n(\cos\theta)$, and $\tau_n(\cos\theta)$.

Inserting the expression of $S(0, r) = S_1(0, r) = S_2(0, r)$ into Eq. (3), we can obtain a well-defined form of the extinction cross section as [8]

$$C_{\mathrm{t}}(r) = \frac{\lambda^2}{2\pi} \sum_{n=1}^{\infty} (2n+1) \mathrm{Re} \left\{ \frac{a_n(r) + b_n(r)}{\eta_{\mathrm{m}}^2} \right\}. \tag{28}$$

For the scattering cross section, no simple closed-form formula is available. It is generally approximated by [9], [10]

$$C_{\mathrm{s}}(r) = \frac{\lambda^2 e^{-4\pi r \mathrm{Im}\{\eta_{\mathrm{m}}\}/\lambda}}{2\pi\gamma|\eta_{\mathrm{m}}|^2} \sum_{n=1}^{\infty} (2n+1) \left( |a_n(r)|^2 + |b_n(r)|^2 \right) \tag{29}$$

with $\gamma = 2(1 + (\beta - 1)e^{\beta})/\beta^2$ and $\beta = 4\pi r \mathrm{Im}\{\eta_{\mathrm{m}}\}/\lambda$. The notation $\mathrm{Re}$ and $\mathrm{Im}$ take the real and imaginary part of a complex number, respectively. The phase function is given by [11]

$$f_{\mathrm{p}}(\theta, r) = \frac{|S_1(\theta, r)|^2 + |S_2(\theta, r)|^2}{4\pi \sum_{n=1}^{\infty} (2n+1)(|a_n(r)|^2 + |b_n(r)|^2)}. \tag{30}$$

## APPENDIX B
## DERIVATION OF $C_{\mathrm{t}}(r)$ IN EQ. (12)

Substituting Eq. (11) into Eq. (3), we have

$$\begin{aligned} C_{\mathrm{t}}(r) &= \frac{4\pi}{|k|^2} \mathrm{Re} \left( S_{\mathrm{D},j}(0, r) + \sum_{p=0}^{\infty} S_j^{(p)}(0, r) \right) \\ &= \frac{4\pi}{|k|^2} \mathrm{Re} \left( \frac{\alpha^2}{2} + \sum_{p=0}^{\infty} \alpha \epsilon_j(0) \sqrt{\frac{1}{4(p/\eta - 2)^2}} e^{\mathrm{i}\phi} \right) \\ &= \frac{4\pi}{|k|^2} \mathrm{Re} \left( \frac{\alpha^2}{2} + \sum_{p\in\mathcal{P}} \alpha \epsilon_j(0) \sqrt{\frac{1}{4(p/\eta - 2)^2}} \cos(\phi) \right) \\ &= 2\pi r^2 + \frac{2\pi r}{|k|} \sum_{p\in\mathcal{P}} \frac{\epsilon_j(0)}{|p/\eta - 1|} \cos\phi \end{aligned} \tag{31}$$

in which $\mathcal{P} = \{1, 3, 5, \cdots\}$.

## APPENDIX C
## GOA FOR PARTICLES WITH ABSORPTION

For particles with absorption, the refractive index is a complex number, which could be written as $\eta_{\mathrm{p}} = \eta_{\mathrm{r}} + \eta_{\mathrm{i}}\mathrm{i}$. Defining the effective refractive index [12]:

$$\begin{aligned} \eta' = \Big\{ & \frac{1}{2}(\eta_{\mathrm{r}}^2 - \eta_{\mathrm{i}}^2 + \eta_{\mathrm{m}}^2 \sin^2\theta_{\mathrm{i}}) \\ & + \frac{1}{2}[4\eta_{\mathrm{r}}^2\eta_{\mathrm{i}}^2 + (\eta_{\mathrm{r}}^2 - \eta_{\mathrm{i}}^2 - \eta_{\mathrm{m}}^2 \sin^2\theta_{\mathrm{i}})^2]^{\frac{1}{2}} \Big\}^{\frac{1}{2}} \end{aligned} \tag{32}$$

we have

$$\eta_{\mathrm{m}} \sin\theta_{\mathrm{i}} = \eta' \sin\theta'_{\mathrm{t}} \tag{33}$$

where $\theta'_{\mathrm{t}}$ is the effective refractive angle. When particles are absorbing, the refractive angle $\theta_{\mathrm{t}}$ should be replaced by $\theta'_{\mathrm{t}}$. The overall phase shift is changed to

$$\phi = \begin{cases} \phi_{\mathrm{p}} + \phi_{\mathrm{f}} + \phi_{\mathrm{r},j} & p = 0 \\ \phi_{\mathrm{p}} + \phi_{\mathrm{f}} + \phi_{\mathrm{t},j} & p > 0 \end{cases} \quad j = 1, 2. \tag{34}$$

The analytical expressions of phase shifts due to reflection $\phi_{\mathrm{r},j}$ and refraction $\phi_{\mathrm{t},j}$ are provided in [12].

Moreover, the amplitude functions in Eq. (7) should be multiplied with the attenuation factor $\xi_p$ [12]:

$$\xi_p = e^{-2\chi p\alpha \cos^2\theta'_{\mathrm{t}}/\eta_{\mathrm{m}}} \tag{35}$$

considering amplitude attenuation in the absorbing particle. Here, $\chi$ is the effective absorption coefficient defined as

$$\chi = \left\{ \frac{1}{2}(-\eta_\mathrm{r}^2 + \eta_\mathrm{i}^2 + \eta_\mathrm{m}^2 \sin^2\theta_\mathrm{i}) + \frac{1}{2}[4\eta_\mathrm{r}^2\eta_\mathrm{i}^2 + (\eta_\mathrm{r}^2 - \eta_\mathrm{i}^2 - \eta_\mathrm{m}^2 \sin^2\theta_\mathrm{i})^2]^{\frac{1}{2}} \right\}^{\frac{1}{2}}. \tag{36}$$

## Appendix D
## Derivation of the Transmittance in Eq. (18)

Considering a light ray $\mathbf{x} \to \mathbf{y}$ passing through a discrete participating medium, the transmittance between $\mathbf{x}$ and $\mathbf{y} = \mathbf{x} - s\boldsymbol{\omega}$ is calculated by

$$\begin{aligned} T(\mathbf{x},\mathbf{y}) &= \exp\left\{ -\int_0^s \sigma_\mathrm{t}(\mathcal{V}_{\mathbf{x}-s'\boldsymbol{\omega}})\mathrm{d}s' \right\} \\ &= \exp\left\{ -\int_0^s \frac{\int_{r_\mathrm{min}}^{r_\mathrm{max}} C_\mathrm{t}(r) \int_{\mathbf{x}\in\mathcal{V}_{\mathbf{x}-s'\boldsymbol{\omega}}} N(r,\mathbf{x})\mathrm{d}\mathbf{x}\mathrm{d}r}{\mu(\mathcal{V}_{\mathbf{x}-s'\boldsymbol{\omega}})} \mathrm{d}s' \right\} \\ &= \exp\left\{ -\int_0^s \frac{\int_{r_\mathrm{min}}^{r_\mathrm{max}} C_\mathrm{t}(r) \int_{\mathbf{x}\in\mathcal{A}\times\mathrm{d}s'} N(r,\mathbf{x})\mathrm{d}\mathbf{x}\mathrm{d}r}{\mu(\mathcal{A}) \times \mathrm{d}s'} \mathrm{d}s' \right\} \\ &= \exp\left\{ -\frac{\int_{r_\mathrm{min}}^{r_\mathrm{max}} C_\mathrm{t}(r) \int_{\mathbf{x}\in\mathcal{A}\times s} N(r,\mathbf{x})\mathrm{d}\mathbf{x}\mathrm{d}r}{\mu(\mathcal{A})} \right\}. \end{aligned} \tag{37}$$

Here we set $\mathcal{V}_{\mathbf{x}-s'\boldsymbol{\omega}}$ to $\mathcal{A} \times \mathrm{d}s'$.

## Appendix E
## More Discussions on $p$

In GOA, the parameter $p$ is the number of chords that each ray makes inside the particle. The ray is internal reflected $p-1$ times before leaving the particle. Since higher-order rays ($p > 3$) have negligible light intensities as compared with other lower-order rays ($p \leq 3$), they can be removed in the computation of the scattering amplitude functions $S_1$ and $S_2$. To validate this, we plot $(|S_1| + |S_2|)/2$ with increasing values of $p$ in Fig. 2 for $\eta = 1.33$ and in Fig. 3 for $p = 1.40$. As see, when $p$ is small (i.e., $p = 1$), the simulated $(|S_1|+|S_2|)/2$ curves have remarkable differences compared with the ground truths generated with a very high order (i.e., $p = 100$). However, the $(|S_1| + |S_2|)/2$ curves with $p = 3$ and $p = 4$ are almost identical, and closely match the ground truths. This implies that $p = 3$ is sufficient in computing $S_1$ and $S_2$ with GOA.

For evaluating the extinction cross section $C_\mathrm{t}$, we can further reduce $p$ to 1. This simplification will lower the computational cost while introducing negligible error, as verified in Fig. 1. Here, we adopt the Relative Mean Squared Error (RelMSE) between $p = 3$ and $p = 1$:

$$\mathrm{RelMSE}\{C_\mathrm{t}\} = \frac{\left(C_\mathrm{t}^{p=3} - C_\mathrm{t}^{p=1}\right)^2}{\left(C_\mathrm{t}^{p=3}\right)^2} \tag{38}$$

to measure the error of $C_\mathrm{t}$. As seen, the RelMSE of $C_\mathrm{t}$ is very low, especially for $r > 1$ $\mu$m.

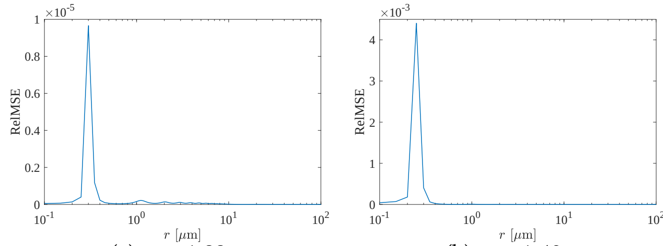


(a) $\eta = 1.33$ (b) $\eta = 1.40$

Fig. 1. Variation of $C_\mathrm{t}$'s RelMSE as a function of the radius $r$.

## Appendix F
## More Comparisons between GOA and Lorenz-Mie Theory

This section provides more visual comparisons between GOA and Lorenz-Mie theory. In Fig. 4, we visualize the curves of $\log S_1(\theta)$ generated by GOA (red curves) and Lorenz-Mie theory (blue curves), respectively. Here, we test two different relative refractive indexes: $\eta = 1.49$ and $\eta = 1.56$. The particle radius ranges from 0.1 $\mu$m to 100 $\mu$m. Again, close agreements are found when $r > 1$ $\mu$m with some differences existing mainly on the backward peaks. When $r = 0.1$ $\mu$m, large errors occur in any direction, indicating that GOA does not work properly in this case. Similar conclusions are reached when comparing GOA and Lorenz-Mie theory for the generation of $\log S_2(\theta)$ curves in Fig. 5.

Although there are some mismatches between GOA and Lorenz-Mie theory in the case of $r = 2$ $\mu$m, the influence on the appearance of rendered media is subtle. To see this, we render a smooth cubic medium in Fig. 6 and Fig. 7 with different scene configurations. The medium is assumed to comprise monodisperse particles. The extinction coefficient and the phase function are respectively determined by Lorenz-Mie theory and GOA in a preprocessing stage, according to the particle radius $r$ and the particle number $N$. However, for $r = 0.1$ $\mu$m we use the same extinction coefficient derived from Lorenz-Mie theory in both cases since GOA yields a negative value. This guarantees the fairness of comparison. Nonetheless, quite different appearances are achieved by Lorenz-Mie theory and GOA when $r = 0.1$ $\mu$m due to the large discrepancy in $S_1(\theta)$ and $S_2(\theta)$. The difference of translucent appearance becomes less noticeable when $r$ goes up to 2 $\mu$m and shrinks further as $r$ increases.

## References


[1] L. Lorenz, "Lysbevægelser i og uden for en af plane lysbølger belyst kugle," *Det kongelig danske Videnskabernes Selskabs Skrifter*, pp. 2–62, 1890.

[2] G. Mie, "Beiträge zur optik trüber medien, speziell kolloidaler metallösungen," *Annalen der Physik*, vol. 330, no. 3, pp. 377–445, 1908.

[3] H. Rushmeier, "Input for participating media," in *ACM SIGGRAPH 1995 Courses*, ser. SIGGRAPH '95, 1995.

[4] P. Callet, "Pertinent data for modelling pigmented materials in realistic rendering," *Computer Graphics Forum*, vol. 15, no. 2, pp. 119–127, 1996.

[5] D. Jackèl and B. Walter, "Modeling and rendering of the atmosphere using mie-scattering," *Computer Graphics Forum*, vol. 16, no. 4, pp. 201–210, 1997.

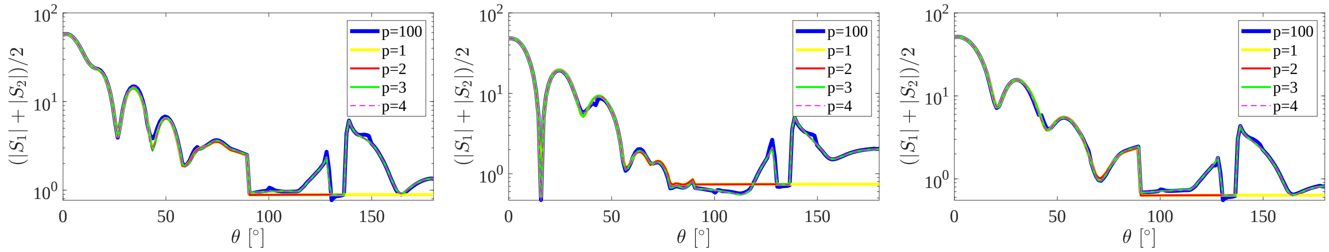


(a) $r = 1$ $\mu$m, $\lambda = 0.5$ $\mu$m (b) $r = 1$ $\mu$m, $\lambda = 0.6$ $\mu$m (c) $r = 1$ $\mu$m, $\lambda = 0.7$ $\mu$m

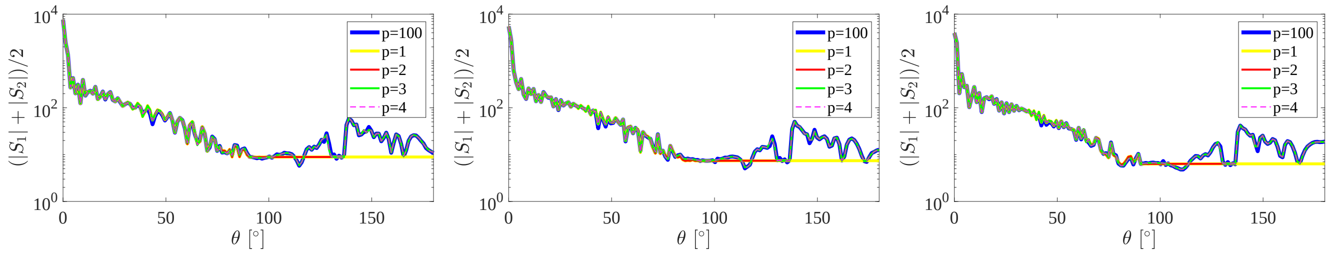


(d) $r = 10$ $\mu$m, $\lambda = 0.5$ $\mu$m (e) $r = 10$ $\mu$m, $\lambda = 0.6$ $\mu$m (f) $r = 10$ $\mu$m, $\lambda = 0.7$ $\mu$m

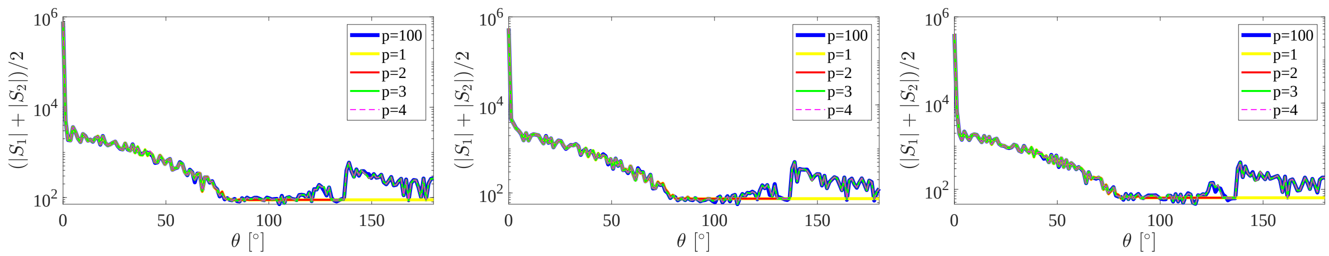


(g) $r = 100$ $\mu$m, $\lambda = 0.5$ $\mu$m (h) $r = 100$ $\mu$m, $\lambda = 0.6$ $\mu$m (i) $r = 100$ $\mu$m, $\lambda = 0.7$ $\mu$m

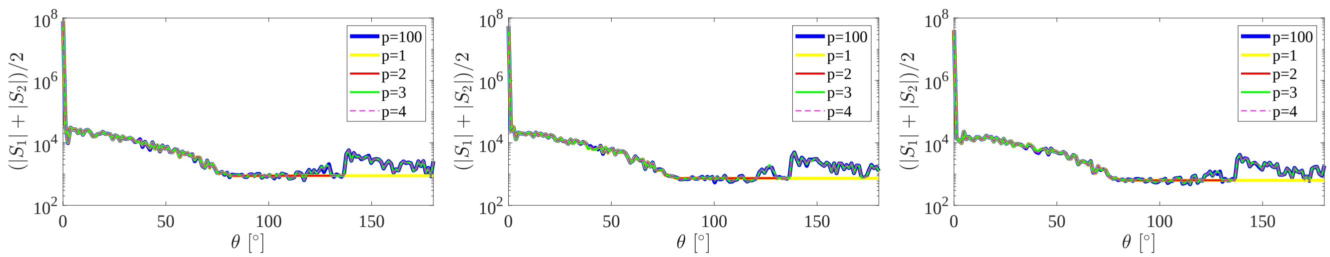


(j) $r = 1000$ $\mu$m, $\lambda = 0.5$ $\mu$m (k) $r = 1000$ $\mu$m, $\lambda = 0.6$ $\mu$m (l) $r = 1000$ $\mu$m, $\lambda = 0.7$ $\mu$m

Fig. 2. Visual comparisons of $(|S_1| + |S_2|)/2$ with increasing values of $p$ in GOA. Here, we show different combinations of particle size $r$ and wavelength $\lambda$, while the relative refractive index of the particle $\eta$ is set to 1.33.

[6] K. Riley, D. S. Ebert, M. Kraus, J. Tessendorf, and C. Hansen, "Efficient rendering of atmospheric phenomena," in *Proceedings of the Fifteenth Eurographics Conference on Rendering Techniques*, ser. EGSR'04, 2004, pp. 375–386.
[7] J. R. Frisvad, N. J. Christensen, and H. W. Jensen, "Computing the scattering properties of participating media using lorenz-mie theory," in *ACM SIGGRAPH 2007 Papers*, ser. SIGGRAPH '07, 2007.
[8] C. F. Bohren and D. P. Gilra, "Extinction by a spherical particle in an absorbing medium," *Journal of Colloid and Interface Science*, vol. 72, no. 2, pp. 215 – 221, 1979.
[9] J. Randrianalisoa, D. Baillis, and L. Pilon, "Modeling radiation characteristics of semitransparent media containing bubbles or particles," *J. Opt. Soc. Am. A*, vol. 23, no. 7, pp. 1645–1656, Jul 2006.
[10] J. Yin and L. Pilon, "Efficiency factors and radiation characteristics of spherical scatterers in an absorbing medium," *J. Opt. Soc. Am. A*, vol. 23, no. 11, pp. 2784–2796, Nov 2006.
[11] H. C. van de Hulst, *Light scattering by small particles*. Dover, 1981.
[12] H. Yu, J. Shen, and Y. Wei, "Geometrical optics approximation for light scattering by absorbing spherical particles," *Journal of Quantitative Spectroscopy and Radiative Transfer*, vol. 110, no. 13, pp. 1178 – 1189, 2009.

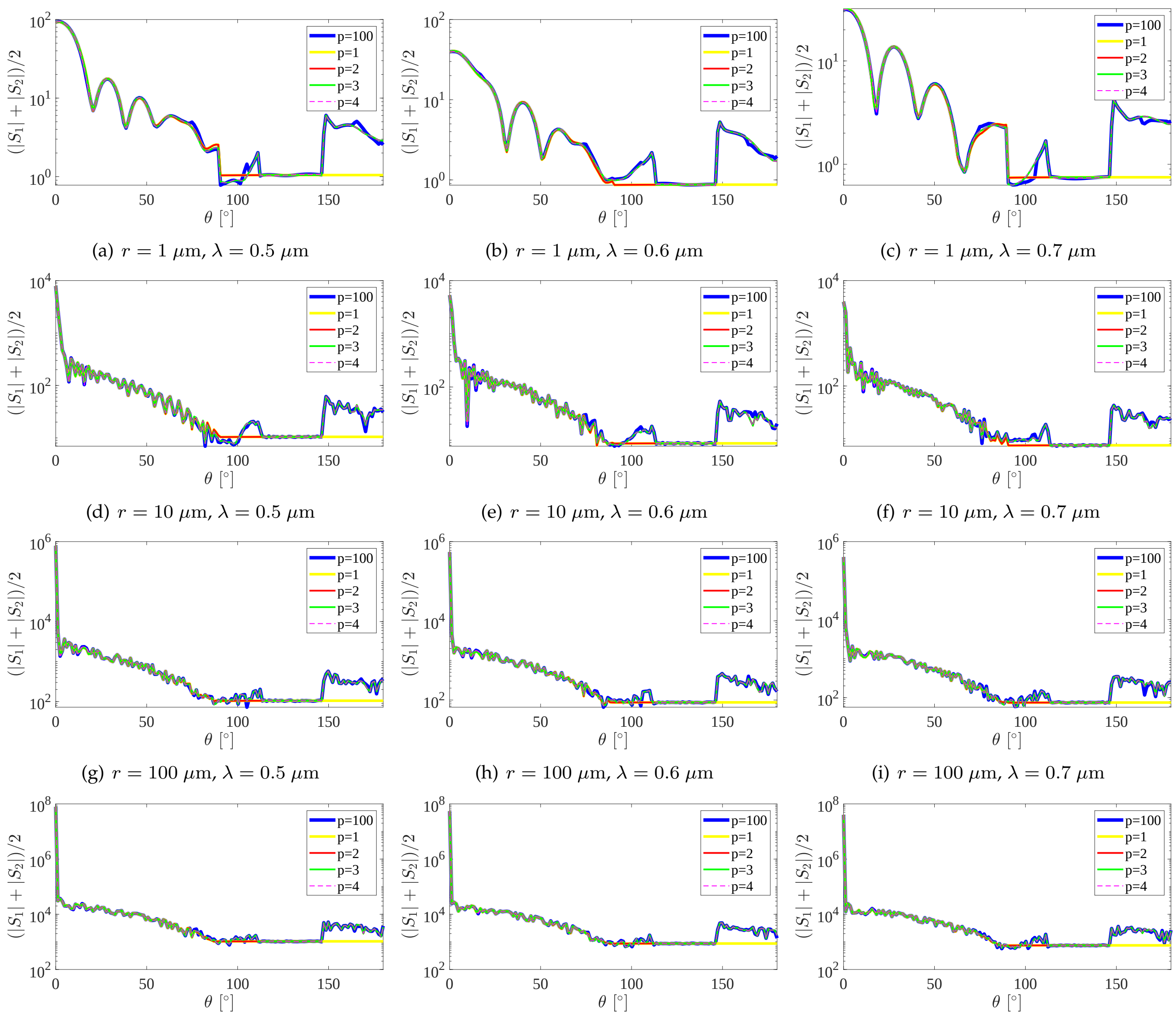


(a) $r = 1\ \mu$m, $\lambda = 0.5\ \mu m$ (b) $r = 1\ \mu$m, $\lambda = 0.6\ \mu m$ (c) $r = 1\ \mu$m, $\lambda = 0.7\ \mu m$

(d) $r = 10\ \mu$m, $\lambda = 0.5\ \mu m$ (e) $r = 10\ \mu$m, $\lambda = 0.6\ \mu m$ (f) $r = 10\ \mu$m, $\lambda = 0.7\ \mu m$

(g) $r = 100\ \mu$m, $\lambda = 0.5\ \mu m$ (h) $r = 100\ \mu$m, $\lambda = 0.6\ \mu m$ (i) $r = 100\ \mu$m, $\lambda = 0.7\ \mu m$

(j) $r = 1000\ \mu$m, $\lambda = 0.5\ \mu m$ (k) $r = 1000\ \mu$m, $\lambda = 0.6\ \mu m$ (l) $r = 1000\ \mu$m, $\lambda = 0.7\ \mu m$

Fig. 3. Visual comparisons of $(|S_1| + |S_2|)/2$ with increasing values of $p$ in GOA. Here, we show different combinations of particle size $r$ and wavelength $\lambda$, while the relative refractive index of the particle $\eta$ is set to 1.40.

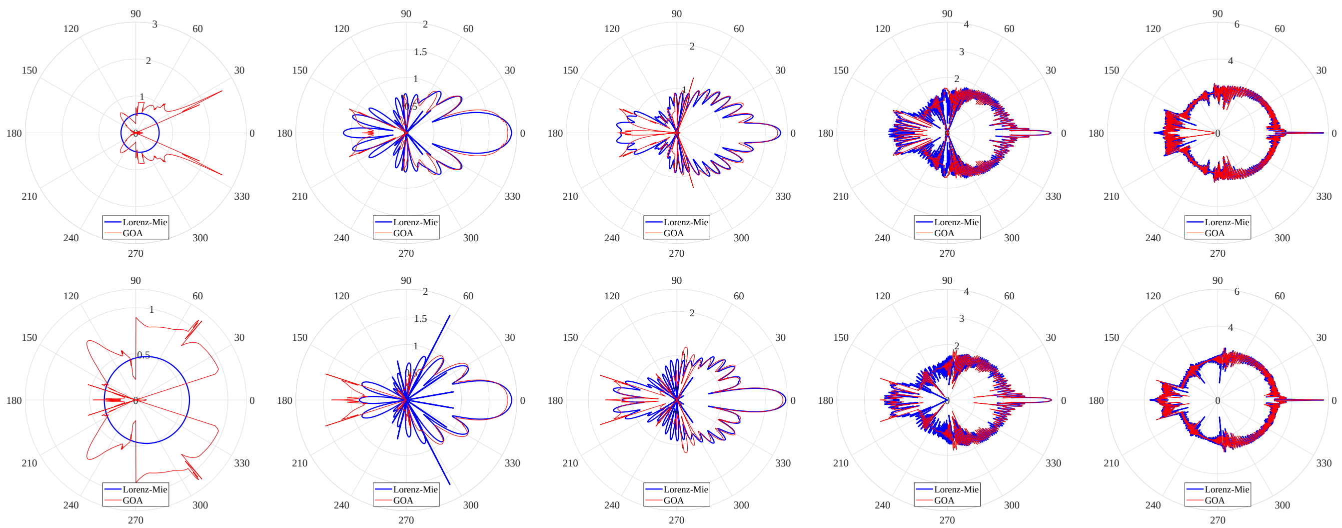


(a) $r = 0.1\ \mu$m (b) $r = 1\ \mu$m (c) $r = 2\ \mu$m (d) $r = 10\ \mu$m (e) $r = 100\ \mu$m

Fig. 4. Visual comparisons of $\log|S_1|$ by Lorenz-Mie calculations (blue curves) with those by GOA (red curves). First row: $\eta = 1.49$ and $\lambda = 0.6\ \mu\mathrm{m}$. Second row: $\eta = 1.56$ and $\lambda = 0.6\ \mu\mathrm{m}$. The particle radius is set to $r = 0.1, 1, 2, 10$ and $100\ \mu\mathrm{m}$, respectively.

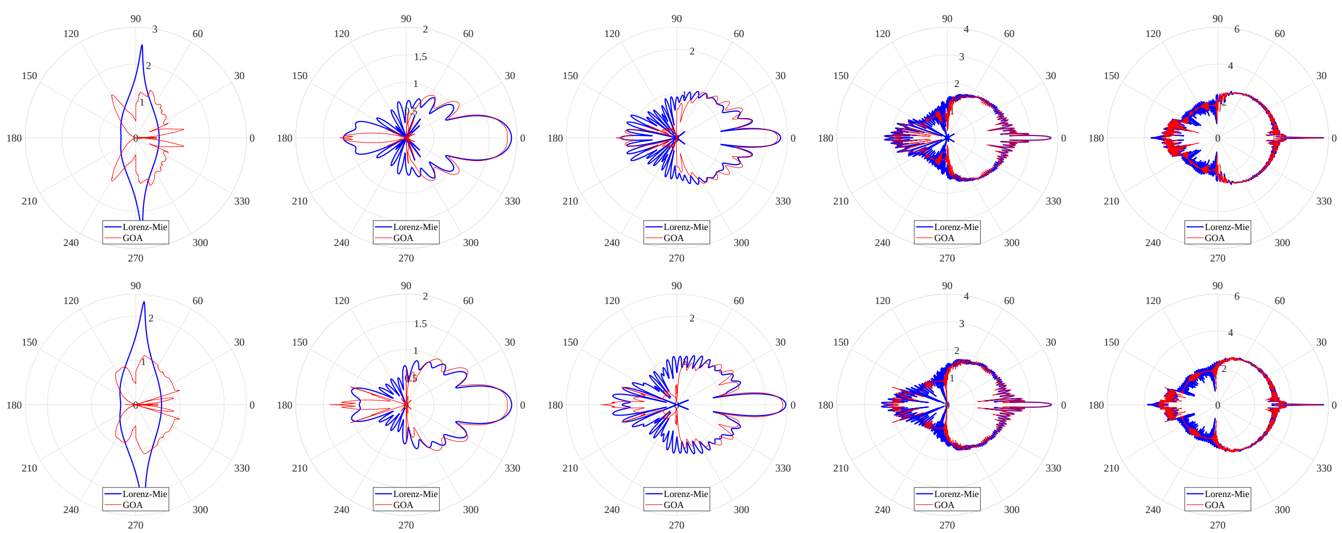


(a) $r = 0.1\ \mu$m (b) $r = 1\ \mu$m (c) $r = 2\ \mu$m (d) $r = 10\ \mu$m (e) $r = 100\ \mu$m

Fig. 5. Visual comparisons of $\log|S_2|$ by Lorenz-Mie calculations (blue curves) with those by GOA (red curves). First row: $\eta = 1.49$ and $\lambda = 0.6\ \mu\mathrm{m}$. Second row: $\eta = 1.56$ and $\lambda = 0.6\ \mu\mathrm{m}$. The particle radius is set to $r = 0.1, 1, 2, 10$ and $100\ \mu\mathrm{m}$, respectively.

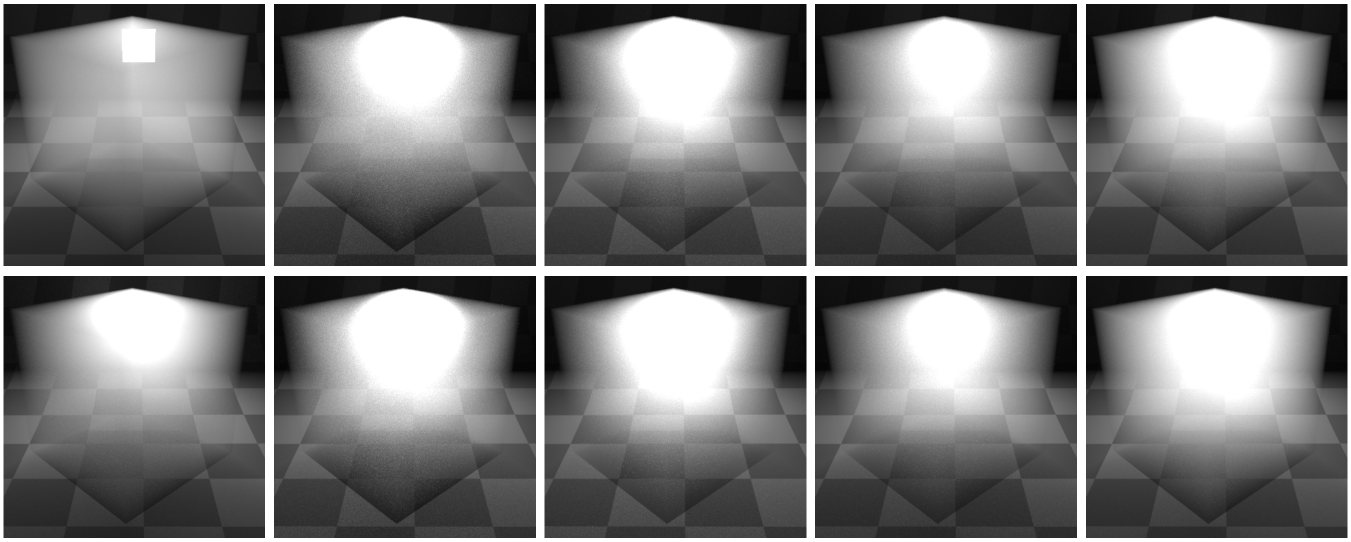

(a) $r = 0.1\ \mu\text{m}$, $N = 10^{14}$ (b) $r = 1\ \mu\text{m}$, $N = 10^{11}$ (c) $r = 2\ \mu\text{m}$, $N = 2 \cdot 10^{10}$ (d) $r = 10\ \mu\text{m}$, $N = 10^{9}$ (e) $r = 100\ \mu\text{m}$, $N = 10^{7}$

Fig. 6. Rendering a smooth cubic medium with optical quantities derived from Lorenz-Mie theory (top row) and GOA (bottom row), respectively. Here, the relative refractive index $\eta$ is set to $1.49$.

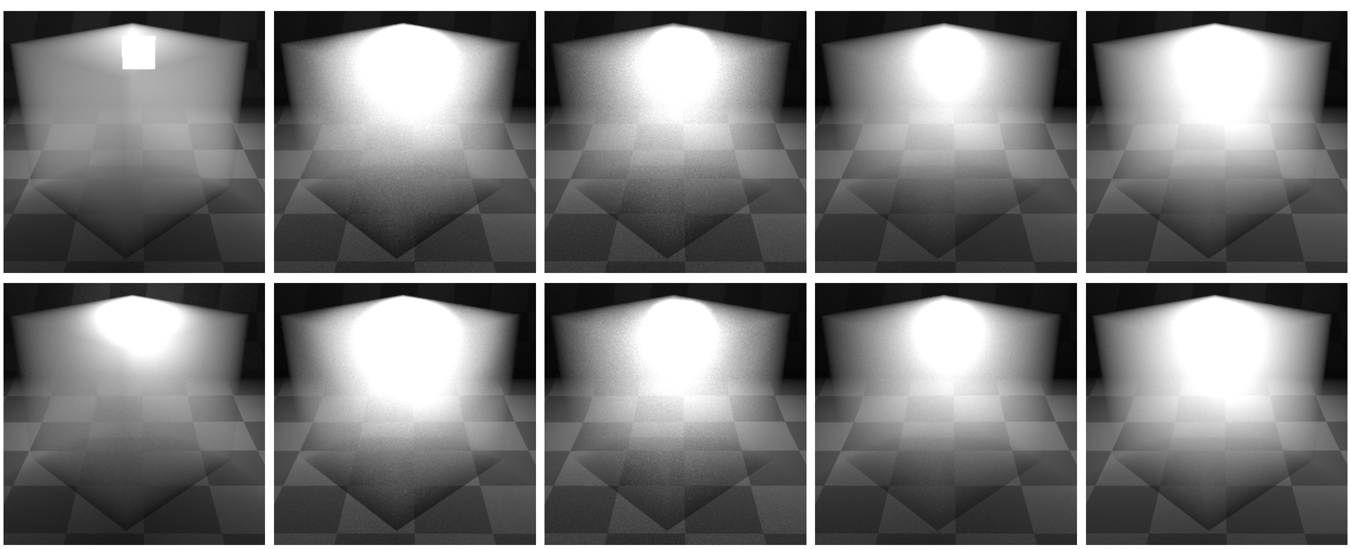

(a) $r = 0.1\ \mu\text{m}$, $N = 10^{14}$ (b) $r = 1\ \mu\text{m}$, $N = 10^{11}$ (c) $r = 2\ \mu\text{m}$, $N = 2 \cdot 10^{10}$ (d) $r = 10\ \mu\text{m}$, $N = 10^{9}$ (e) $r = 100\ \mu\text{m}$, $N = 10^{7}$

Fig. 7. Rendering a smooth cubic medium with optical quantities derived from Lorenz-Mie theory (top row) and GOA (bottom row), respectively. Here, the relative refractive index $\eta$ is set to $1.56$.